CLINICAL ARTICLE

Motor Bur Milling State Identification via Fast Fourier Transform Analyzing Sound Signal in Cervical Spine Posterior Decompression Surgery

He Bai, MD[1†] , Rui Wang, MD[1†], Qiu Wang, MD[2†], Guang-ming Xia, PhD[3] , Yuan Xue, PhD[1] , Yu Dai, PhD[3], Jian-xun Zhang, PhD[3]

Department of [1]Orthopaedics Surgery and [2]Rehabilitation, Tianjin Medical University General Hospital and [3]Tianjin Key Laboratory of Intelligent Robotics, College of Computer and Control Engineering, Institute of Robotics and Automatic Information System, Nankai University, Tianjin, China

Objectives: To investigate the real-time sensitive feedback parameter of the motor bur milling state in cervical spine posterior decompression surgery, to possibly improve the safety of cervical spine posterior decompression and robot-assisted spinal surgeries.

Methods: In this study, the cervical spine of three healthy male and three healthy female pigs were randomly selected. Six porcine cervical spine specimens were fixed to the vibration isolation system. The milling state of the motor bur was defined as the lamina cancellous bone (CA), lamina ventral corticalbone (VCO), and penetrating ventral cortical bone (PVCO). A 5-mm bur milled the CA and VCO, and a 2-mm bur milled the VCO and PVCO. A miniature microphone was used to collect the sound signal (SS) of milling lamina which was then extracted using Fast Fourier Transform (FFT). When using 5-mm and 2-mm bur to mill, the CA, VCO, and PVCO of each specimen were continuously collected at 1, 2, 3, 4, 5, 6, 7, 8, 9, and 10 kHz frequencies for SS magnitudes. The study randomly selected the SS magnitudes of the CA and VCO continuously for 2 s at 1, 2, 3, 4, and 5 kHz frequencies for statistical analyses. When milling the VCO to the PVCO, we randomly collected the SS magnitudes of the VCO for consecutive 2 s and the SS magnitudes of continuous 2 s in the penetrating state at 1, 2, 3, 4, and 5 kHz frequencies for statistical analyses. The independent sample *t*-test was used to compare the SS magnitudes of different milling states extracted from the FFT to determine the motor bur milling state.

Results: The SS magnitudes of the CA and VCO of all specimens extracted from the FFT at 1, 2, and 3 kHz were statistically different ($P < 0.01$); three specimens were not statistically different at a specific FFT-extracted frequency (first specimen at 5 kHz, SS magnitudes of the CA were $[25.94 \pm 8.74] \times 10^{-3}$, SS magnitudes of the VCO were $[28.67 \pm 12.94] \times 10^{-3}$, $P = 0.440$; second specimen at 4 kHz, SS magnitudes of the CA were $[23.79 \pm 7.94] \times 10^{-3}$, SS magnitudes of the VCO were $[24.78 \pm 4.32] \times 10^{-3}$, $P = 0.629$; and third specimen at 5 kHz, SS magnitudes of the CA were $[16.76 \pm 6.20] \times 10^{-3}$, SS magnitudes of the VCO were $[17.69 \pm 6.44] \times 10^{-3}$, $P = 0.643$). The SS magnitudes of the VCO and PVCO of all the specimens extracted from the FFT at each frequency were statistically different ($P < 0.001$).

Conclusions: Based on the FFT extraction, the SS magnitudes of the motor bur milling state between the CA and VCO, the VCO and PVCO were significantly different, confirming that the SS is a potential sensitive feedback parameter

Address for correspondence Yuan Xue, PhD, Department of Orthopaedics Surgery, Tianjin Medical University General Hospital, 154 Anshan Road, Heping District, Tianjin, China 300052 Tel: +8613512003188; Fax: +860222721952; Email: xueyuanzyy@163.com
Yu Dai, PhD, Institute of Robotics and Automatic Information System, Tianjin Key Laboratory of Intelligent Robotics, College of Computer and Control Engineering, Nankai University, 94 Weijin Road, Nankai District, Tianjin, China 300071 Tel: +8615022500382; Fax: +860222721952; Email: daiyu@nankai.edu.cn
†These authors contributed equally to this work

for identifying the motor bur milling state. This study could improve the safety of cervical spine posterior decompression surgery, especially of robot-assisted surgeries.

Key words: Cervical spine decompression; Cervical spine laminectomy; Fast Fourier Transform; Milling lamina sound signal; Motor bur milling state

Introduction

Cervical spondylotic myelopathy is the most common cause of quadriplegia in adults[1,2]. For adults over 50 years of age, the cause of paralysis is primarily cervical spinal stenosis leading to spinal cord dysfunction; surgical decompression is considered the only effective procedure for treating patients with cervical spondylotic myelopathy[3,4]. Cervical spine posterior decompression is accepted as a treatment option for posterioror multilevel cord compression[5–7]. The two most common posterior cervical spine decompression procedures are cervical laminoplasty and laminectomy[8]. In both procedures, the lamina cancellous bone (CA) and lamina ventralcortical bone (VCO) should be milled using a motor bur to open or remove the lamina. However, neurological complications (NLCL) after posterior cervical spine decompression have always been a clinical conundrum, occurring in approximately 6% of patients[9,10].

Piezosurgery is currently considered to be safe, has great cutting precision, and does not resonate with nerve tissues[11,12]. However, some technical challenges associated with piezosurgery are difficult to address. First, the energy continues to transmit after the lamina has been cut by the piezosurgery saw, causing the adjacent tissue (e.g. spinal cord) to vibrate; this may cause NLCL. Second, the saw of piezosurgery is in the spinal canal and cannot be viewed directly. Third, the saw of piezosurgery can squeeze or cause thermal injury to the dura and nerve tissues. The advantages of the motor bur are as follows: first, the milling process is always performed under direct vision; second, if the surgeon ensures that the motor bur does not touch the dura during the operation, the spinal cord function will be preserved[13]. Therefore, the motor bur is still an irreplaceable power device for bone milling in spine surgery, especially in spinal canal stenosis[14].

The motor bur may slip during the operation due to surgeon hand tremor or fatigue, leading to severe NLCL[15]. Somatosensory-evoked potentials[16,17], motor-evoked potentials[18], and electromyography recordings[19,20] are applied as the spinal cord and nerve injury monitor in most spine surgeries, but the above monitoring methods lag behind in spinal cord and nerve injuries caused by the motor bur. Exploring a sensitive parameter for monitoring the motor bur milling state, which could provide real-time feedback immediately after the VCO is penetrated, will help in avoiding complications from the spinal cord and nerve injures caused by the motor bur during cervical spine posterior decompression surgery.

Robotic assistance in spinal surgery provides many benefits for the patient, surgical staff, and surgeon; it is associated with lower intraoperative complications[21–23]. Robotic systems allow the surgeon three-dimensional visualizations of the patient's imaging and also enable the surgical team to view the operation remotely via telesurgery[24–26]. Nevertheless, intraoperative navigation is also challenging in patients with spinal deformities and spinal canal stenosis. In spinal stenosis, the space between the bone and spinal cord is reduced, and the nerve tissues are delicate. If the bone structure boundary cannot be sensitively identified to control the movement of the motor bur during the lamina milling process, it will easily cause the motor bur to deviate or slip from the original coordinate path, which could lead to spinal cord and nerve tissue injuries.

The development of robotic assistance to improve spine surgery safety is currently restricted to navigation[27,28]. Recent studies have demonstrated that robotic assistance is potentially engaged in more complex spine surgeries such aspercutaneous vertebroplasty or deformity correction. However, lamina milling requires maintaining the stiffness and freedom of the bur and accurately identifying the boundaries of the bone structures, which is still a technical challenge in the development of operational spine surgery robots.

Several techniques based on biomechanical factors, bioelectrical impedance, haptic (force and vibration), and electrical power feedback have been studied[29–33]. The significance is that when there is a deviation of a specific feedback parameter during the operation, if other feedback parameters alter in time and the operation is disrupted, the safety and stability of robot-assisted spine surgery could be increased. Currently, there is ongoing research on the addition of the identification of feedback parameters to the identification of the milling state of the motor bur in robot-assisted spine surgery. Force feedback of spine-assistant robots have been studied, and they can identify the milling state of the motor bur more accurately; however, the force sensor can only be fixed on the non-rotating structure of the power tool. The signal-to-noise ratio is low, and the force sensor is expensive and disposable. Theoretically, it does not have the potential for milling state recognition. Our previous study investigated the sound signal (SS) feature[34], which aids trajectory determination and screw implantation[35]. To date, there have been no reports on the use of Fast Fourier Transform (FFT) in the extraction of the SS in lamina milling to determine the milling state of the motor bur in cervical spine posterior decompression surgery.

The purpose of this study was threefold. The first was to extract the SS of the milling lamina using the FFT, compare the SS magnitudes at different frequencies, and make

the compound SS comparable. The second was to propose a feedback parameter of real-time non-contact motor bur milling states (including the CA, VCO, and penetratingventral cortical bone [PVCO]) based on FFT extractionin cervical spine posterior decompression surgery. The final was to provide a feedback parameter to improve the safety of cervical spine posterior decompression surgery, especially of robot-assisted surgeries.

Methods

Specimen Preparation and Surgical Procedures

Six fresh cervical spine specimens were harvested from 6-month-old pigs (weight range, 25–32 kg; three females and three males). All the specimens underwent a two-step surgical procedure. First, the spinous processes and all nonessential soft tissues were carefully dissected to preserve the facet joint capsules and ligamentous structures. The specimen was then fixed to the operating table (DAEIL SYSTEMS, Vibration Isolation Systems, Yongin Korea) usinga chucking fixture. Second, the operation power system GD676 (B. Braun company, Tuttlingen, Germany) was used to mill the lamina on C5. A 5-mm diameter bur was engaged vertically (Y-axis) to mill the CA and VCO. A 2-mm bur was applied to vertically penetrate the VCO (Fig. 1). The vertical downward movement speed of the robotic arm was set to 0.2 mm/s. The bur was washed with 0.9% normal saline during the milling process, at a flow of approximately 30 mL/min. The experiments were performed according to the guidelines for animal care and were approved by the Animal Ethics Committee.

Motor Bur and Operation Power System

The high-speed operation power system GD676 (B. Braun company, Tuttlingen, Germany), which allowed rotation of 10,000 to 80,000 revolutions per minute (rpm), was chosen for the experiment, and the spindle speed of the motor was set at 60,000 rpm. Two mellow burs (Stryker Corporation, Kalamazoo, Michigan, USA) with diameters of 5 and 2 mm were applied separately.

Sound Signal Collection

The motor bur was installed on a three-axis motion control platform driven by a stepping motor, and X, Y, and Z were three mutually perpendicular linear motion axes. The stepping motor used an OMAP-L137 DSP (Texas Instruments, Texas, USA) as the system controller. The SS was collected using a 46BE free-field microphone (GRAS, Holte, Denmark) and a USB-4431 dynamic signal acquisition module (National Instruments, Austin, USA). The microphone was installed to the side of the milling device, 100 ± 2 mm from the bur (Fig. 2). The microphone had a workspace of 10–40 KHz (which covered the range of human hearing) and a resolution of 4 mV/Pa. The dynamic signal acquisition module provided a 24-bit analog-to-digital converter with a maximum sampling frequency of 102.4 kHz.

Sound Signal Extraction Using the FFT

At the point when the motor burs the lamina, the dynamic milling force $F(t)$ is:

$$F(t) = F_0 + \sum_{n=1}^{L} F_n \sin(2\pi n f_r t + \varphi_n), \tag{1}$$

where f_r is the rotation frequency of the spindle of the high-speed operation power system, F_n represents the amplitude of the nth milling harmonic force, φ_n is the initial phase angle ofthe nth milling harmonic force, and F_0 is the magnitude of the direct-current constant force. In this study, only the first five frequencies were used for motor bur milling state identification because the SS magnitudes at the high-order frequencies were relatively small, thus, $L = 5$.

Assuming that the lamina being milled is relatively rigid and the muscles and ligaments are flexible, the dynamic model of the cervical spine is considered a single-degree-of-freedom system in the feed direction (Fig. 3); therefore, the vibration equation can be formulated as follows:
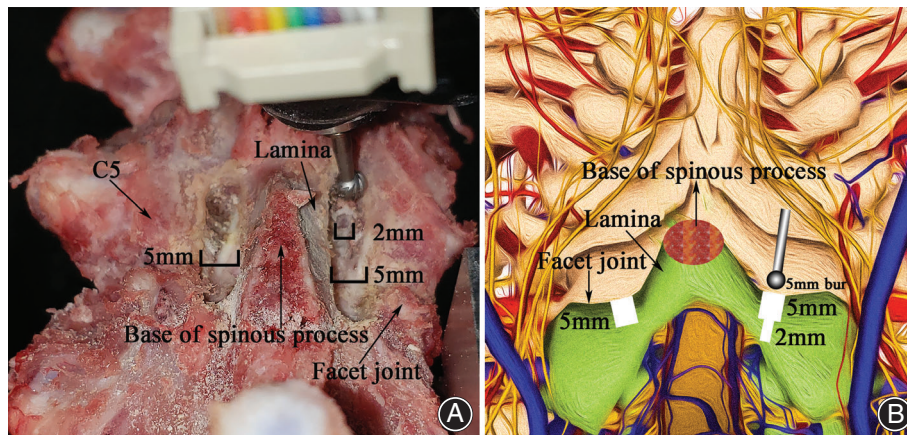

Fig. 1 The 5-mm and 2-mm bur milling processes in experiment (A). Corresponding sketch map (B).
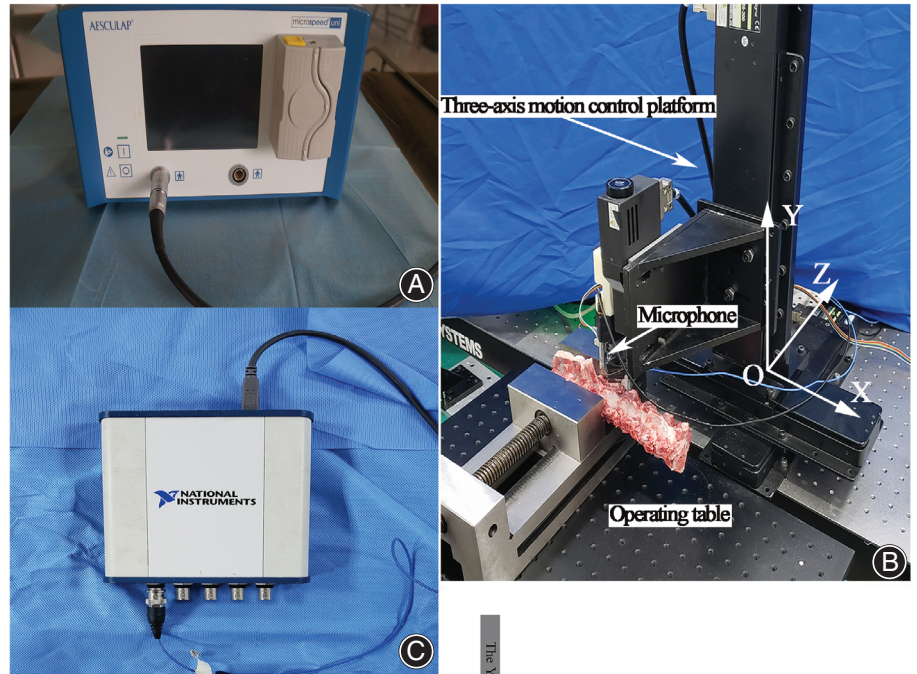
Fig. 2 High-speed operation power system GD676 (B. Braun company, Tuttlingen, Germany) (A). Three-axis motion control platform, 46BE free-field microphone (GRAS, Holte, Denmark), operating table (DAEIL SYSTEMS, Vibration Isolation Systems, Yongin Korea) (B). USB-4431 dynamic signal acquisition module (National Instruments, Austin, USA) (C). Sketch map of the SS collection (D).
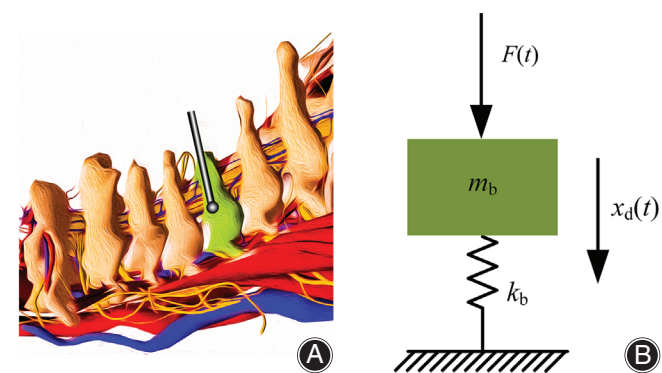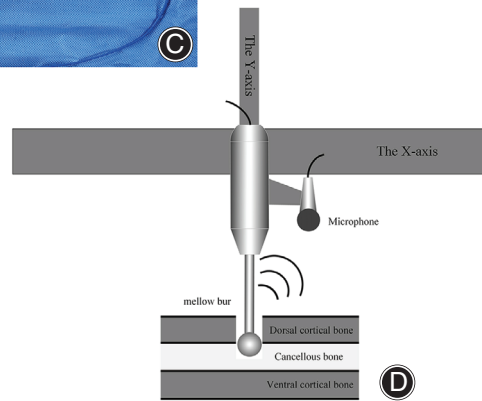

Fig. 3 The dynamic model of the cervical spine and milling device (A). $F(t)$ is the dynamic milling force, m_b is the equivalent mass of the musculoskeletal system, $x_d(t)$ is the displacement of the mass m_b from the equilibrium position, k_b is the equivalent stiffness of the musculoskeletal system (B).

$$m_b \frac{d^2 x_d(t)}{dt^2} + k_b x_d(t) = F(t), \tag{2}$$

where m_b and k_b represent the equivalent mass and stiffness of the musculoskeletal system, respectively.

The displacement of the equivalent mass m_b from the equilibrium position is $x_d(t)$, which is calculated as follows:

$$x_d(t) = \frac{F_0}{k_b} + \sum_{n=1}^{L} \frac{F_n \sin\left(2\pi n f_r t + \varphi'_n\right)}{k_b\left(1 - \lambda_n^2\right)}, \tag{3}$$

where λ_n is the ratio of the frequency of the nth milling harmonic force to the natural frequency ω_n of the musculoskeletal system and φ'_n is the initial phase angle of the nth milling harmonic force,

$$\lambda_n = \frac{2\pi n f_r}{\omega_n}, \tag{4}$$

Fig. 4 FFT extracted the SS during the CA milling process. The 5-mm bur milled the CA (4—0). The SS of six specimens (4—1) — (4—6) during 5-mm bur milling. FFT randomly 0.1s extracted the SS magnitudes (4—1′) — (4—6′) from (4—1) — (4—6), respectively.
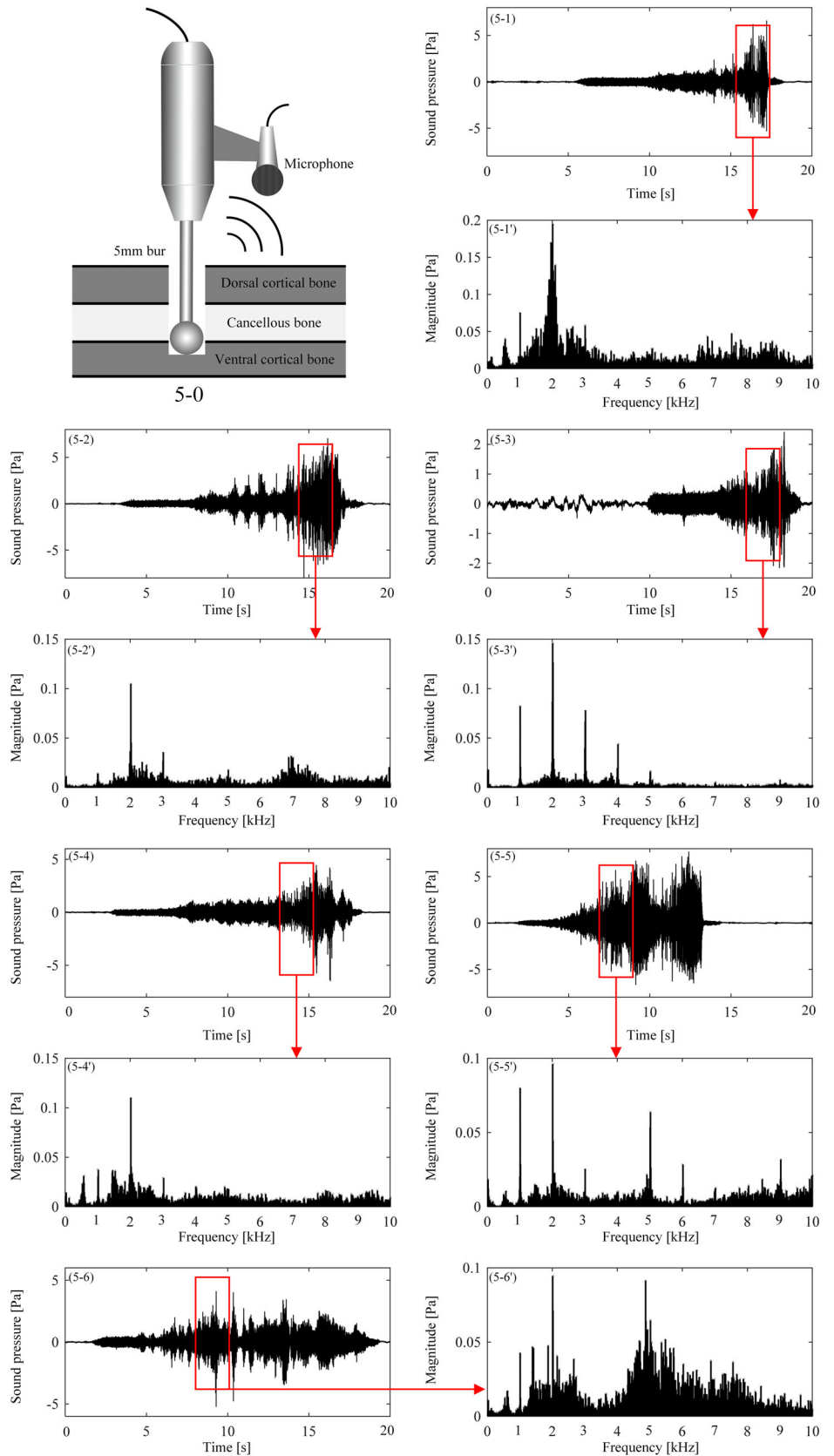
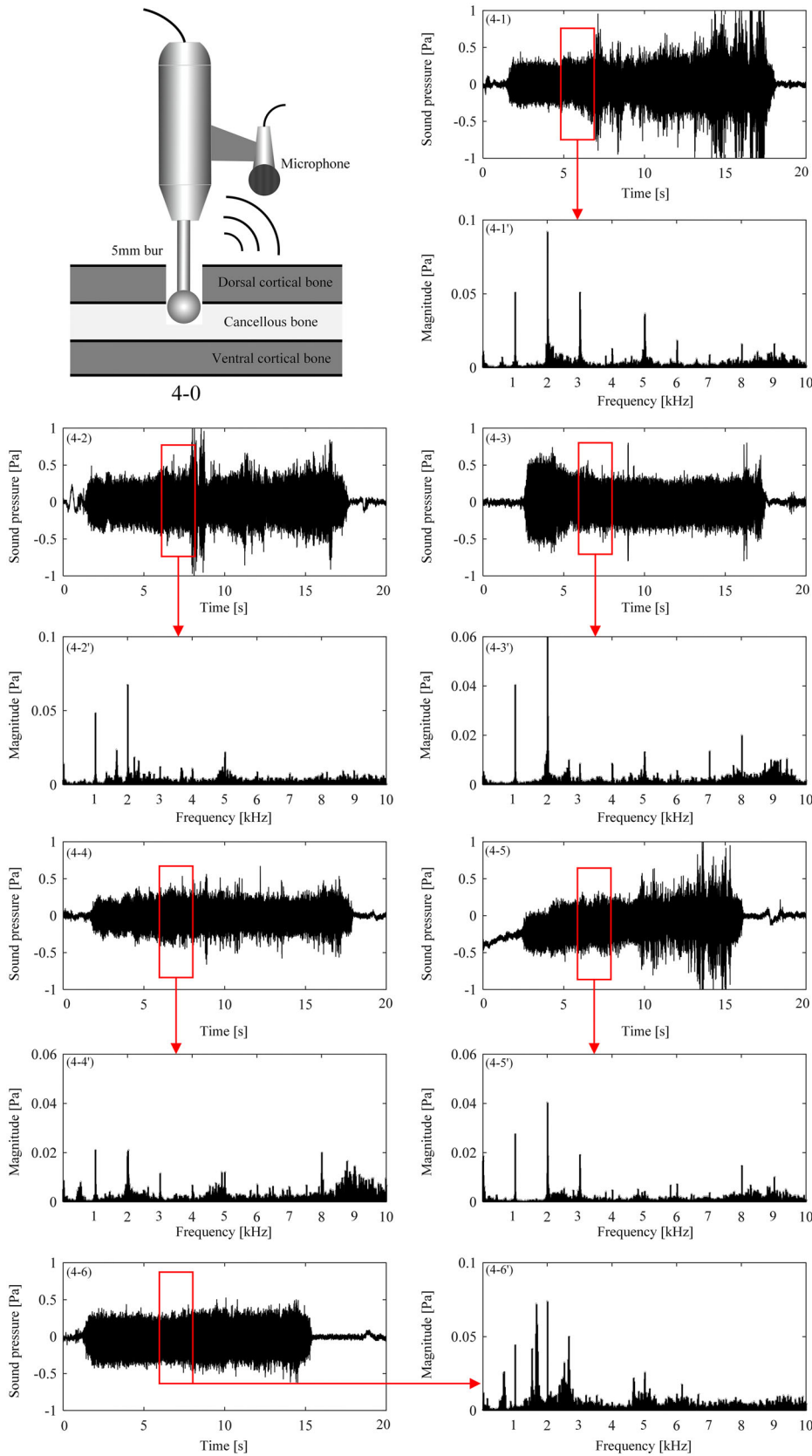**Fig. 5** FFT extracted the SS during the VCO milling process. The 5-mm bur milled the VCO (5—0). The SS of six specimens (5—1) — (5—6) during 5-mm bur milling. FFT randomly 0.1 s extracted the SS magnitudes (5—1′) — (5—6′) from (5—1) — (5—6), respectively.

Fig. 6 FFT extracted the SS from VCO milling to penetration. The 2-mm bur milled the VCO (6—0). The SS of six specimens (6—1) — (6—6) during 2-mm bur milling. FFT randomly 0.1 s extracted the SS magnitudes (6—1′) — (6—6′) from (6—1) — (6—6), respectively.

Fig. 7 FFT extracted the SS from VCO milling to penetration. The 2-mm bur milled the PVCO (7—0). The SS of six specimens (7—1) — (7—6) during 2-mm bur milling penetration. FFT randomly 0.1 s extracted the SS magnitudes (7—1′) — (7—6′) from (7—1) — (7—6), respectively.
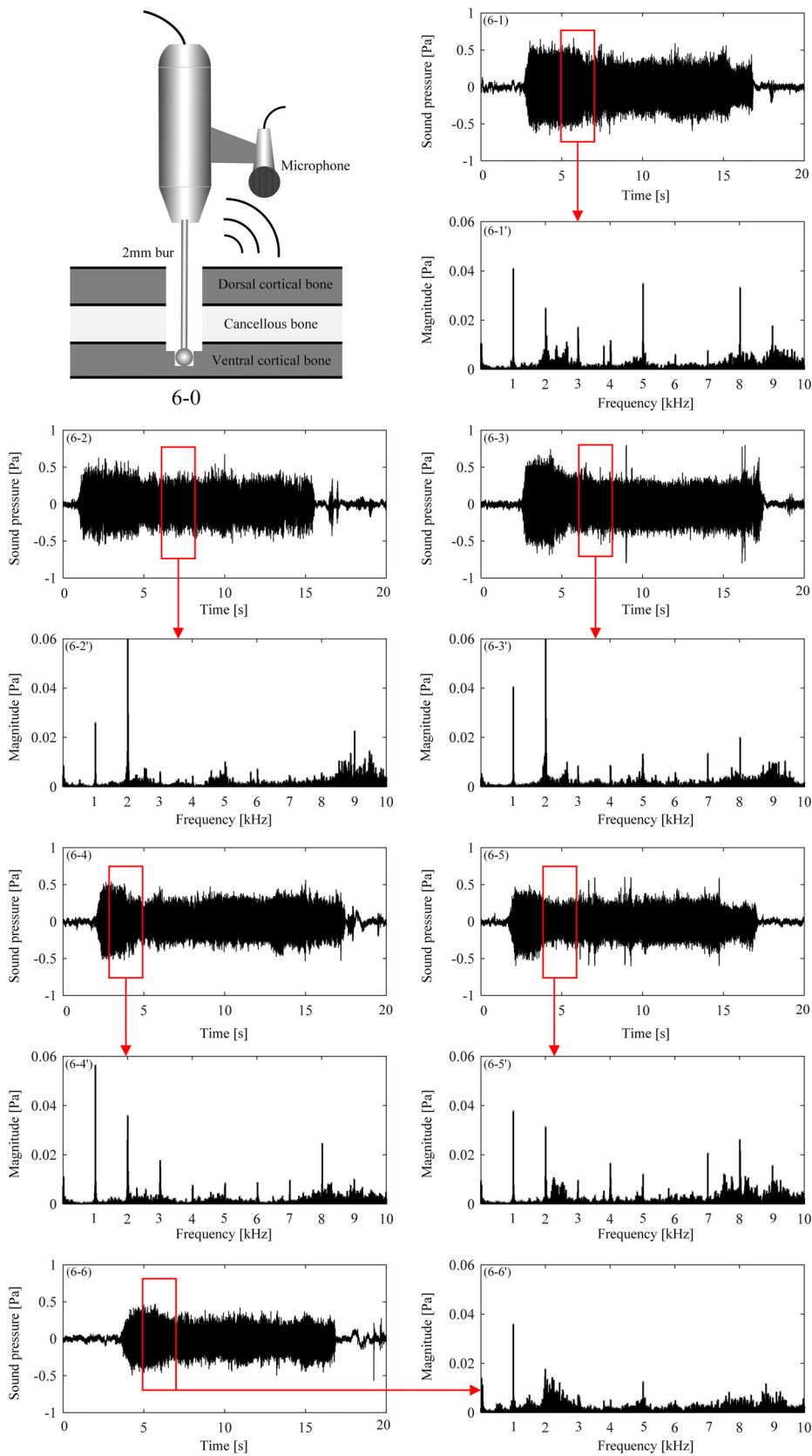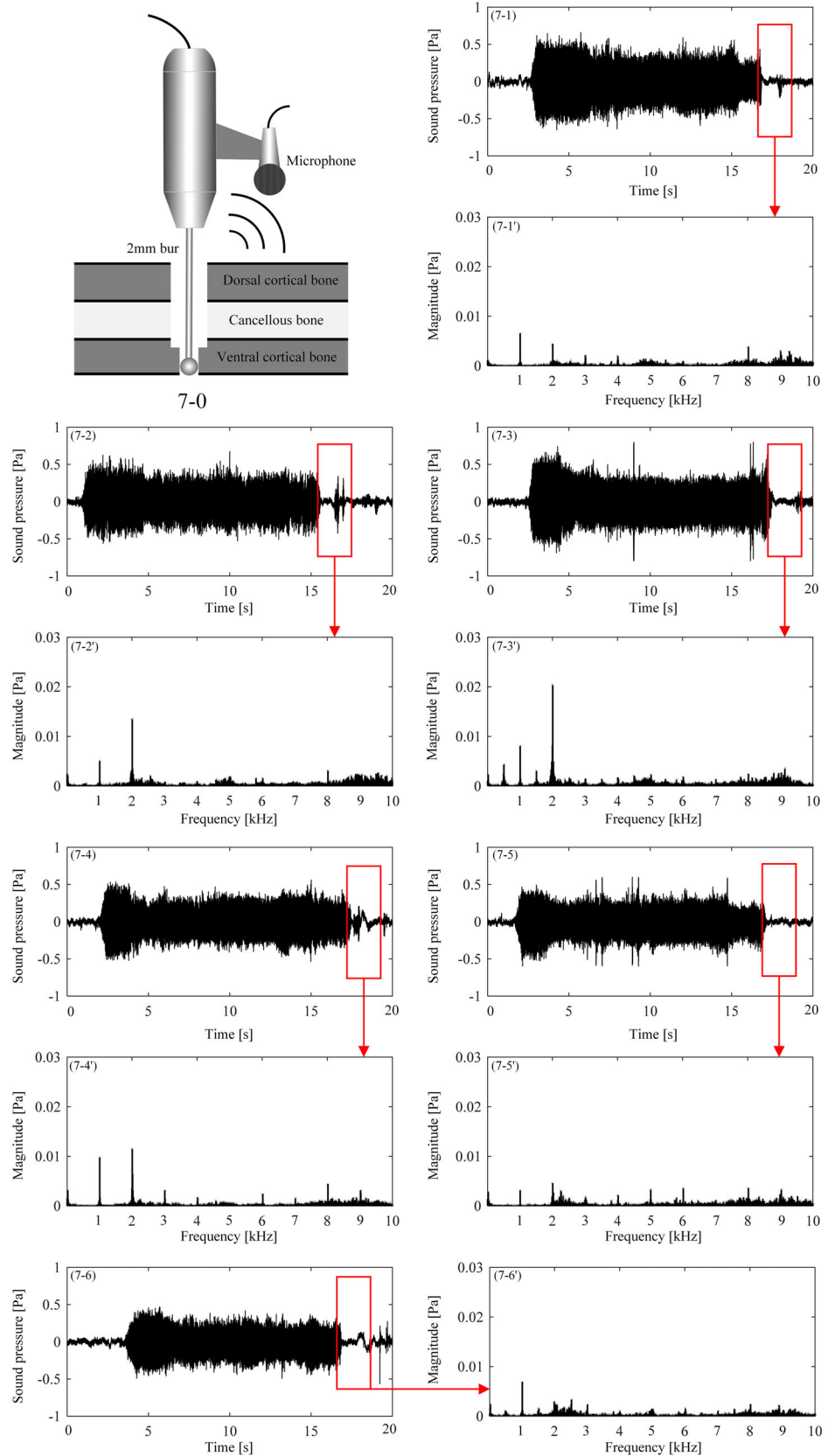
TABLE 1 FFT extraction outcomes (mean ±SD) in specimens (1–6) of 5-mm bur milling

Specimen	Milling state (5-mm bur)	Frequency [Hz]				
		1000	2000	3000	4000	5000
1	CA	38.34 ± 7.43	110.21 ± 21.45	28.51 ± 8.54	6.24 ± 2.47	25.94 ± 8.74
	VCO	100.28 ± 13.85	263.70 ± 84.24	73.75 ± 27.90	14.15 ± 4.66	28.67 ± 12.94
2	CA	31.26 ± 6.86	75.39 ± 38.30	11.34 ± 4.80	23.79 ± 7.94	18.12 ± 7.78
	VCO	42.47 ± 6.79	373.04 ± 229.33	49.02 ± 16.98	24.78 ± 4.32	32.95 ± 7.60
3	CA	40.26 ± 12.48	47.27 ± 25.22	11.86 ± 4.59	7.85 ± 3.42	16.76 ± 6.20
	VCO	89.81 ± 4.82	216.33 ± 64.02	64.20 ± 15.64	40.56 ± 8.94	17.69 ± 6.44
4	CA	17.02 ± 5.75	33.50 ± 18.04	18.60 ± 5.72	12.46 ± 6.67	14.04 ± 4.36
	VCO	51.30 ± 8.14	208.97 ± 72.89	27.48 ± 10.62	84.55 ± 18.60	248.33 ± 139.53
5	CA	56.70 ± 11.87	39.11 ± 17.98	6.72 ± 1.84	5.80 ± 1.85	19.16 ± 7.27
	VCO	67.05 ± 9.24	315.63 ± 73.48	49.40 ± 22.60	45.41 ± 17.97	71.97 ± 29.09
6	CA	31.48 ± 11.46	82.50 ± 16.28	26.46 ± 8.54	8.16 ± 2.23	27.16 ± 9.89
	VCO	81.00 ± 23.12	306.10 ± 131.47	39.40 ± 7.68	47.56 ± 14.62	57.23 ± 14.97

All (mean ± standard deviation) multiplied by 10^{-3}

TABLE 2 FFT extraction outcomes (mean ± standard deviation) in specimens (1–6) of 2-mm bur milling

Specimen	Milling state (2-mm bur)	Frequency [Hz]				
		1000	2000	3000	4000	5000
1	VCO	31.04 ± 5.67	192.19 ± 9.30	6.83 ± 1.60	4.06 ± 1.23	10.62 ± 3.08
	PVCO	0.84 ± 0.70	1.12 ± 2.60	0.55 ± 0.90	0.48 ± 0.67	0.56 ± 1.13
2	VCO	45.69 ± 9.94	89.36 ± 18.16	10.22 ± 5.06	5.48 ± 2.28	16.74 ± 6.19
	PVCO	1.67 ± 2.94	0.68 ± 0.74	0.46 ± 0.46	0.35 ± 0.19	0.27 ± 0.07
3	VCO	60.05 ± 28.73	76.26 ± 47.69	13.54 ± 4.58	12.34 ± 2.97	19.56 ± 9.03
	PVCO	0.63 ± 0.49	0.80 ± 1.60	0.58 ± 1.02	0.41 ± 0.50	0.61 ± 1.08
4	VCO	37.59 ± 10.90	173.16 ± 40.74	21.06 ± 3.65	10.90 ± 2.54	12.78 ± 6.52
	PVCO	0.86 ± 0.65	0.63 ± 0.60	0.43 ± 0.16	0.36 ± 0.08	0.34 ± 0.13
5	VCO	43.40 ± 9.72	172.66 ± 33.53	11.47 ± 4.76	7.26 ± 2.18	10.02 ± 6.20
	PVCO	0.57 ± 0.54	0.95 ± 1.92	0.40 ± 0.50	0.34 ± 0.29	0.44 ± 0.49
6	VCO	30.61 ± 15.95	89.11 ± 43.13	17.60 ± 6.27	3.06 ± 0.92	11.21 ± 5.84
	PVCO	0.73 ± 0.68	1.19 ± 2.64	0.72 ± 1.04	0.52 ± 0.55	0.71 ± 1.20

All (mean ± standard deviation) multiplied by 10^{-3}.

TABLE 3 The *P* values of pairwise comparison between SS magnitudes extracted by the FFT in different milling states (5- and 2-mm burs)

| Specimen	Milling state		*P* values in different frequency [Hz]				
			1000	2000	3000	4000	5000
1	5-mm bur	CA *vs* VCO	<0.001	<0.001	<0.001	<0.001	0.440
	2-mm bur	VCO *vs* PVCO	<0.001	<0.001	<0.001	<0.001	<0.001
2	5-mm bur	CA *vs* VCO	<0.001	<0.001	<0.001	0.629	<0.001
	2-mm bur	VCO *vs* PVCO	<0.001	<0.001	<0.001	<0.001	<0.001
3	5-mm bur	CA *vs* VCO	<0.001	<0.001	<0.001	<0.001	0.643
	2-mm bur	VCO *vs* PVCO	<0.001	<0.001	<0.001	<0.001	<0.001
4	5-mm bur	CA *vs* VCO	<0.001	<0.001	0.002	<0.001	<0.001
	2-mm bur	VCO *vs* PVCO	<0.001	<0.001	<0.001	<0.001	<0.001
5	5-mm bur	CA *vs* VCO	0.004	<0.001	<0.001	<0.001	<0.001
	2-mm bur	VCO *vs* PVCO	<0.001	<0.001	<0.001	<0.001	<0.001
6	5-mm bur	CA *vs* VCO	<0.001	<0.001	<0.001	<0.001	<0.001
	2-mm bur	VCO *vs* PVCO	<0.001	<0.001	<0.001	<0.001	<0.001

5mm bur
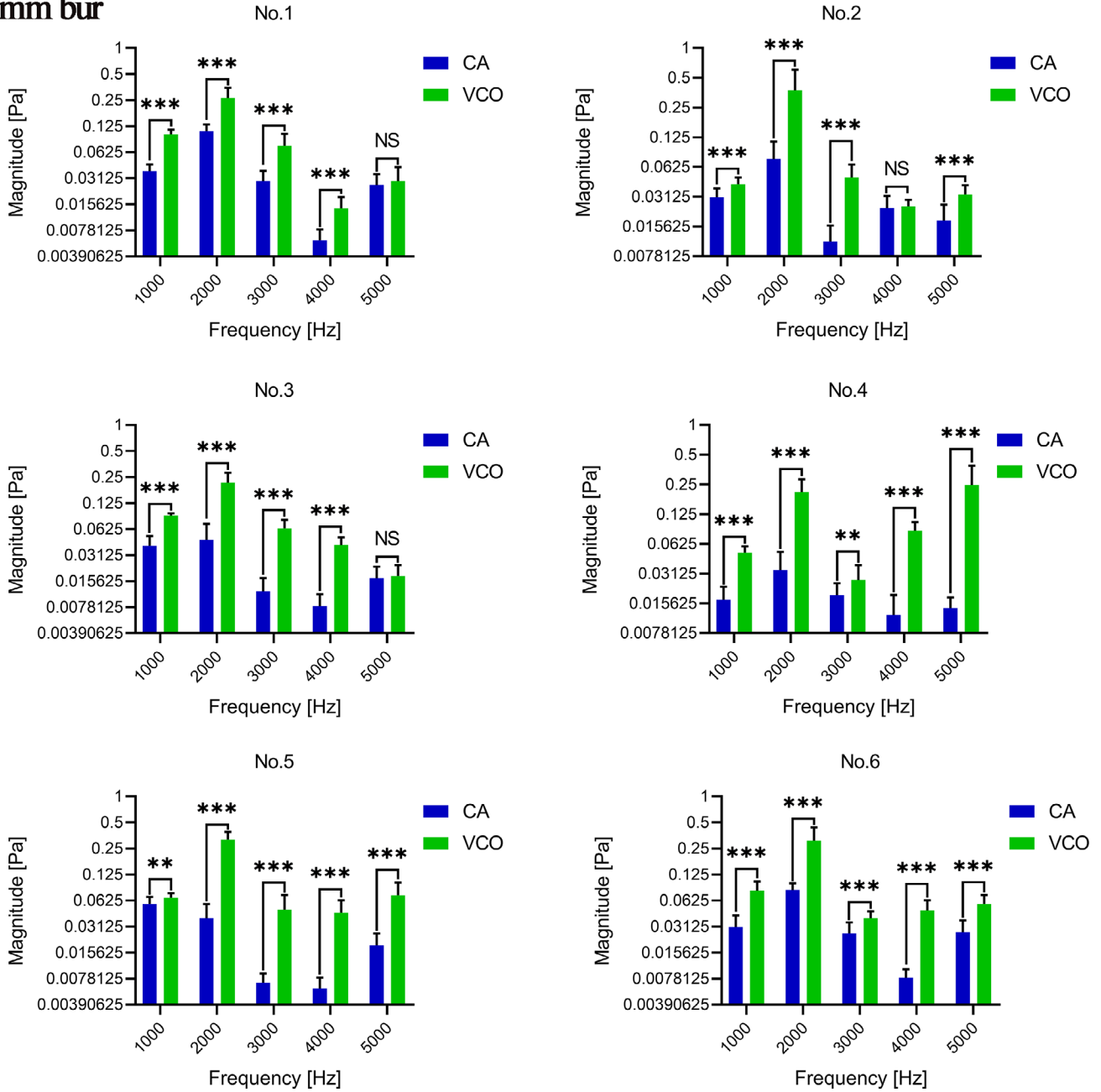
Fig. 8 The statistical difference ($P < 0.01$) of the SS magnitudes between the CA and the VCO extracted by FFT during the 5-mm bur milling. NS indicates no statistical difference.

and

$$\omega_n = \sqrt{\frac{k_b}{m_b}}. \tag{5}$$

The high-speed operation power system GD676 can provide a periodic milling harmonic force. The influencing factors of the F_n mainly included the following: (i)structural characteristics of the motor bur relative to the sharpness of the bur blade, material, and craft; (ii) instantaneous volume of bone removed, which depends on the feed speed of the motor bur; and (iii) the bone density of the lamina in the milling area. Therefore, the empirical exponent formula for F_n is

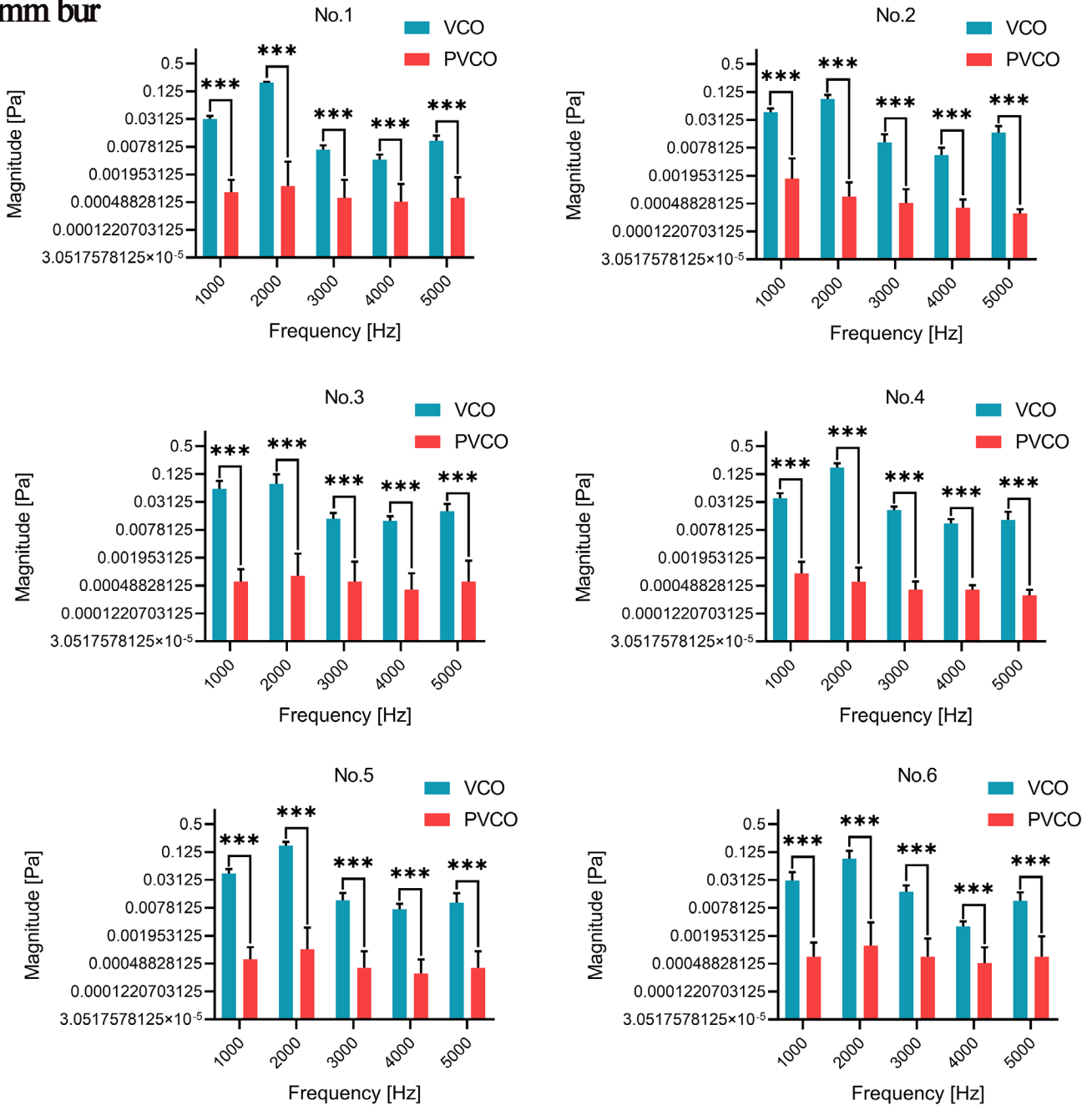$$F_n = \gamma_n \rho^{k_\rho} V^{k_V}, \tag{6}$$

Fig. 9 The statistical difference ($P < 0.001$) of the SS magnitudes between the VCO and PVCO extracted by FFT during the 2-mm bur milling.

where γ_n is the motor bur structure characteristic coefficient of the nth milling harmonic force, ρ is the milling bone density, V is the instantaneous bone removal volume, and k_ρ and k_V are the index coefficients of ρ and V.

The SS was produced by vibrations that occurred when the motor bur was milling the lamina. According to formula (3), the acceleration of $a_b(t)$ of the musculoskeletal system is

calculated using the second derivative of the displacement $x_d(t)$ with respect to time:

$$a_b(t) = \sum_{n=1}^{L} \frac{F_n}{\frac{k_b}{(2\pi n f_r)^2} - m_b} \sin\left(2\pi n f_r t + \varphi'_n\right), \quad (7)$$

the $s(t)$ is the SS which can be expressed as:

$$s(t) = \alpha a_b(t) = \sum_{n=1}^{L} \frac{\alpha F_n}{\frac{k_b}{(2\pi n f_r)^2} - m_b} \sin\left(2\pi n f_r t + \varphi'_n\right), \quad (8)$$

where α is the proportional coefficient of the vibration to sound.

Data Collection and Statistical Analyses

The motor bur milling procedures included the following states: the CA milled by a 5-mm bur, and the VCO milled by a 5- and 2-mm bur (Figs Fig. 4–Fig. 6), and the VCO until the PVCO milled by a 2-mm bur (Fig. 7). The milling was performed only on the contralateral sides of the C5 lamina of each specimen. The SS of the CA, VCO, and PVCO were collected. Subsequently, the FFT of MATLAB (version 8.3, 2019a, USA) was used to extract the SS as SS magnitudes at frequencies of 1, 2, 3, 4, 5, 6, 7, 8, 9, and 10 kHz. We chose to analyze the SS magnitudes at frequencies of 1, 2, 3, 4, and 5 kHz because those of the high-order frequencies were relatively small. The FFT of MATLAB was used to continually extract the SS magnitudes every 0.1 s throughout the milling. When milling with the 5-mm bur, continuous 2s SS magnitudes were randomly selected for statistical analyses. When using a 2-mm bur to mill the VCO to the PVCO, randomly collected the SS magnitudes of the VCO for consecutive 2 s and the SS magnitudes of the continuous 2 s in the PVCO for statistical analyses. The SS extracted during penetration was controlled within 0.1 s, which was sufficient to identify the critical state of penetration in real-time. Determination of the motor burmilling state was performed using the independent sample t-test of SPSS (version 24.0, IBM, USA). Differences were considered statistically significant at $P < 0.05$.

Results

StatisticalAnalyses in the 5- and 2-mm Bur Milling

The robotic arm at a speed of 0.2 mm/s was used to perform a vertically down milling on the C5 lamina of six porcine cervical spine specimens, and the SS of the CA, VCO, and PVCO was successfully obtained. An independent sample t-test was used for the statistical analyses. The mean ($\pm$SD) of SS magnitudes of all the specimens under the different motor bur milling states at each investigated frequency of the FFT are shown in Tables 1 and 2.

Statistical Results of the SS Magnitudes of CA and VCO During the 5-mm Bur Milling

Table 3 and Fig. 8 show that at frequencies of 1, 2, and 3 kHz, the SS magnitudes of the CA and VCO of all the specimens were statistically different ($P < 0.01$). At a frequency of 4 kHz, the SS magnitudes of the CA and VCO of specimen no. 2 were not statistically different ($P > 0.05$); they were statistically different ($P < 0.01$) at the other frequencies. At a frequency of 5 kHz, the SS magnitudes of the CA and

VCO of specimen nos. 1 and 3 were not statistically different ($P > 0.05$); they were statistically different ($P < 0.01$) at the other frequencies.

Results of Statistical Analyses of the SS Magnitudes of VCO and PVCO During the 2-mm Bur Milling

Table 3 and Fig. 9 show that the SS magnitudes of the VCO and PVCO of all the specimens were statistically different ($P < 0.001$) at each frequency. The SS magnitudes of the VCO were larger than those of the PVCO at all frequencies.

Discussion

Extraction of the Statistical Analyses Results of SS Using the FFT

This study investigated the feasibility of applying the FFT to the extraction of the SS of lamina milling for determining the motor bur milling state to improve the safety of milling operation, especially in the milling penetration state during cervical spine posterior decompression surgery. The findings showed that there were statistically significant differences between the SS magnitudes of the CA and VCO of all the specimens at 1, 2, and 3 kHz when the 5-mm bur was used to mill. When using the 2-mm bur to bur, the SS magnitudes of the VCO and PVCO of all the specimens were statistically different at each frequency, confirming that the SS can be used as a real-time sensitive parameter for feedback on the motor bur milling state during cervical spine posterior decompression surgery.

Theory and Outcome of Extracting SS by FFT to Identify the Milling states

In our research, according to equations (6), (7), and (8), the rate of bur advancement is constant, which makes the instantaneous volume of bone removed constant. γ_n is the sharpness of the bur and is related to the material and craft of the bur. The density of the lamina bone (ρ) in the milling area is the only factor affecting the SS magnitudes; therefore, the difference in SS can be used to discriminate the motor bur milling state. It is well-known that SS is extracted by FFT in integer multiples of spindle frequency, and the environment always contains some noise whose frequency is not an integer multiple of spindle frequency[34,35]. Therefore, we excluded the influence of noise in the environment during the experiment. Table 3 and Fig. 8 show that the SS magnitudes of the CA and VCO are statistically different at specific frequencies. Table 3 and Fig. 9 show that the SS magnitudes of the VCO and PVCO are statistically different at each frequency. When PVCO stopped collecting SS, the bur did not wholly plunge into the spinal canal. Because the feed speed of the motor bur along the Y-axis was 0.2 mm/s, and the FFT extraction time was 0.1 s, the critical state of penetration could be identified in real-time.

Comparison of SS Identification Milling States with Previous Study and No Statistical Difference Analyses

Our findings on the use of the SS to identify the milling state during spine surgery are consistent with those of our previous study[34,35]. However, when using the 5-mm bur to mill the lamina, some specimens showed no statistical difference between the CA and VCO at specific frequencies. At a frequency of 4 kHz, the SS magnitudes of the CA and VCO of specimen no. 2 were not statistically different. At a frequency of 5 kHz, the SS magnitudes of the CA and VCO of specimen nos. 1 and 3 were not statistically different, which may have been caused by an experimental deviation during the operation and the short sampling time of the SS. Further studies are required including extensive *in vitro* experiments and experiments on other animals or fresh cadaver specimens.

To Identify the Significance and Advantages of Milling States in Cervical Spine Posterior Decompression Surgery by Using the SS

Cervical spine posterior decompression is considered a high-risk surgery, and laminectomy and unilateral open-door laminoplasty have been the main methods for cervical spine posterior decompression[9,10,36]; both methods involve bone milling to create gutters at the junction between the articular processes and laminae bilaterally[37–39]. To form the hinge of the open door, preservation of the VCO is critical in preventing lamina reclosure. To form the open side and remove the lamina (laminectomy), interrupting the VCO while avoiding contact with the dura is crucial. Therefore, the CA, VCO, and PVCO are essential components of real-time feedback control in laminectomy and laminoplasty surgeries. Due to the lack of reliable feedback on the milling state during cervical spine posterior decompression surgery, decompression operation easily damages the dural sac, spinal cord, and nerves and causes excessive milling to the hinge. Postoperative complications such as acute neurological deterioration, NLCL, paraplegia, and hinge fractures are likely to occur[9,10,15]. In addition, the surgeon's physiological hand tremor and intraoperative fatigue[13,15] increase the risk of postoperative complications. Although some surgeons use the somatosensory-evoked potentials[16,17], motor-evoked potentials[18], and electromyography recordings[19,20] to monitor the safety of decompression during posterior cervical decompression surgery, these monitoring methods cannot provide real-time feedback. The major strength of this study is that the SS could be used as a sensitive feedback parameter, which can help surgeons identify the CA, VCO, and PVCO during cervical spine posterior decompression surgery in real-time, thereby increasing the safety of the operation and reducing the risk and complications from the surgery.

Provide a Valuable Feedback Parameter for Robot-Assisted Spinal Surgeries

The desire to improve the safety and reduce the risks of cervical spine posterior decompression surgery has prompted the emergence of robotics in spinal surgery. Compared with conventional surgical methods, spine-assistant robots are more accurate, stable, and automated[21–23]. However, robot-assisted spine surgery is limited to intraoperative navigation and a few surgical operations (such as pedicle screw placement and percutaneous kyphoplasty) due to the lack of reliable milling feedback parameters[27,28]. Accurately controlling the milling state of the motor bur is still a technical challenge in the development of spine surgery robots. Bioelectrical impedance, haptic (force and vibration), and electrical power feedback have been studied in robot-assisted spine surgery[29–33]. However, these feedback parameters have poor signal-to-noise ratios and are high in cost. In contrast, the SS has the advantages of a high signal-to-noise ratio, real-time feedback, non-contact, and low cost[34,35]. As a reliable and sensitive real-time feedback parameter, SS is expected to increase the safety of robot-assisted spinal surgeries.

Significance and Deficiencies of Study

Our study results suggest that the SS could be a new parameter for providing feedback on the motor bur milling state during cervical spine posterior decompression surgery. This study was associated with several limitations. First, it was an *ex vivo* specimen experiment. The damping effect of the surrounding musculature, fat, and retractors during the milling process was not considered. Second, movement (breathing mobility) may have affected the experimental results. Next, live animal operations will be conducted. The effects of damping and mobility will be addressed by optimizing the calculation from deep learning (AI) based on colossal data collection. Finally, considering that the SS of pathological laminae such as osteosclerosis and osteoporosis have not been measured, the proposed method is only efficient with normal laminae. In the future, we will perform studies on pathological laminae and further verify the validity of our experimental results.

Data Availability

Data are available on request from the corresponding author.

Author Contributions

Conceptualization: Yuan Xue, Yu Dai, and Jianxun Zhang. Data curation: He Bai, Rui Wang, and Qiu Wang. Formal analysis: He Bai, Rui Wang, and Qiu Wang. Writing –original draft: He Bai and Rui Wang. Writing – review and editing: He Bai, Rui Wang, Qiu Wang, Guangming Xia, Yuan Xue, and Yu Dai.

References

1. Singh A, Tetreault L, Casey A, Laing R, Statham P, Fehlings MG. A summary of assessment tools for patients suffering from cervical spondylotic myelopathy: a systematic review on validity, reliability and responsiveness. Eur Spine J, 2015, 24: 209–228.

2. Hirabayashi S, Yamada H, Motosuneya T, *et al*. Comparison of enlargement of the spinal canal after cervical laminoplasty: open-door type and double-door type. Eur Spine J, 2010, 19: 1690–1694.

3. Emery SE, Bohlman HH, Bolesta MJ, Jones PK. Anterior cervical decompression and arthrodesis for the treatment of cervical spondylotic myelopathy. Two to seventeen-year follow-up. J Bone Joint Surg Am, 1998, 80: 941–951.
4. Bakhsheshian J, Mehta VA, Liu JC. Current diagnosis and management of cervical spondylotic myelopathy. Global Spine J, 2017, 7: 572–586.
5. Youssef JA, Heiner AD, Montgomery JR, et al. Outcomes of posterior cervical fusion and decompression: a systematic review and meta-analysis. Spine J, 2019, 19: 1714–1729.
6. Salzmann SN, Derman PB, Lampe LP, et al. Cervical spinal fusion: 16-year trends in epidemiology, indications, and in-hospital outcomes by surgical approach. World Neurosurg, 2018, 113: e280–e295.
7. Huang KT, Harary M, Abd-El-Barr MM, Chi JH. Crossing the cervicothoracic junction following posterior cervical decompression and fusion: a cohort analysis. World Neurosurg, 2019, 131: e514–e520.
8. Lee BJ, Park JH, Jeon SR, Roh SW, Rhim SC, Jung SK. Posterior cervical muscle-preserving interspinous process approach and decompression: more minimally invasive and modified Shiraishi's selective laminectomy. World Neurosurg, 2020, 133: e412–e420.
9. Thirumala PD, Muralidharan A, Loke YK, Habeych M, Crammond D, Balzer J. Value of intraoperative neurophysiological monitoring to reduce neurological complications in patients undergoing anterior cervical spine procedures for cervical spondylotic myelopathy. J Clin Neurosci, 2016, 25: 27–35.
10. Lee MJ, Konodi MA, Cizik AM, et al. Risk factors for medical complication after cervical spine surgery: a multivariate analysis of 582 patients. Spine (Phila Pa 1976), 2013, 38: 223–228.
11. Liu X, Li T, Shi L, et al. Application of Piezosurgery in en bloc laminectomy for the treatment of multilevel thoracic ossification of ligamentum flavum. World Neurosurg, 2019, 126: 541–546.
12. Grauvogel J, Scheiwe C, Kaminsky J. Use of Piezosurgery for removal of retrovertebral body osteophytes in anterior cervical discectomy. Spine J, 2014, 14: 628–636.
13. Praamsma M, Carnahan H, Backstein D, Veillette CJ, Gonzalez D, Dubrowski A. Drilling sounds are used by surgeons and intermediate residents, but not novice orthopedic trainees, to guide drilling motions. Can J Surg, 2008, 51: 442–446.
14. Leimert M, Bostelmann R, Juratli TA, et al. A newly developed drill with a polished tip for the anterior cervical approach in spinal canal stenosis: a technical note. Eur Spine J, 2013, 22: 809–812.
15. Young WF, Baron E. Acute neurologic deterioration after surgical treatment for thoracic spinal stenosis. J Clin Neurosci, 2001, 8: 129–132.
16. Cofano F, Zenga F, Mammi M, et al. Intraoperative neurophysiological monitoring during spinal surgery: technical review in open and minimally invasive approaches. Neurosurg Rev, 2019, 42: 297–307.
17. Oya J, Burke JF, Vogel T, Tay B, Chou D, Mummaneni P. The accuracy of multimodality intraoperative neuromonitoring to predict postoperative neurologic feficits following anterior cervical laminoplasty. World Neurosurg, 2017, 106: 17–25.
18. Takeda M, Yamaguchi S, Mitsuhara T, Abiko M, Kurisu K. Intraoperative neurophysiologic monitoring for degenerative cervical myelopathy. Neurosurg Clin N Am, 2018, 29: 159–167.
19. Ando M, Tamaki T, Matsumoto T, et al. Can postoperative deltoid weakness after cervical laminoplasty be prevented by using intraoperative neurophysiological monitoring. J Clin Monit Comput, 2019, 33: 123–132.
20. Jou IM, Lai KA. Neuromonitoring of an experimental model of clip compression on the spinal nerve root to characterize acute nerve root injury. Spine (Phila Pa 1976), 1998, 23: 932–939 discussion 939–940.
21. D' Souza M, Gendreau J, et al. Robotic-assisted spine surgery: history, efficacy, cost, and future trends. Robot Surg, 2019, 6: 9–23.
22. Feng S, Tian W, Wei Y. Clinical effects of oblique lateral interbody fusion by conventional open versus percutaneous robot-assisted minimally invasive pedicle screw placement in elderly patients. Orthop Surg, 2020, 12: 86–93.
23. Luo J, Yan YJ, Wang XD, Long XD, Lan H, Li KN. Accuracy and safety of robot-assisted drilling decompression for osteonecrosis of the femoral head. Orthop Surg, 2020, 12: 784–791.
24. Zhu J, Sun KQ, Lu LT, et al. Snake-eye screwing: a novel free-hand technique of pedicle screw placement in cervicothoracic spine and preliminary clinical results. Orthop Surg, 2021, 13: 35–44.
25. Tian W, Liu YJ, Liu B, et al. Guideline for posterior atlantoaxial internal fixation assisted by orthopaedic surgical robot. Orthop Surg, 2019, 11: 160–166.
26. Zhang Q, Xu YF, Tian W, et al. Comparison of superior-level facet joint violations between robot-assisted percutaneous pedicle screw placement and conventional open fluoroscopic-guided pedicle screw placement. Orthop Surg, 2019, 11: 850–856.
27. Cao G, Dai Y, Zhang J, Jia B, Ge J. Design of control system for bone drilling robot based on vibration signal feedback. In: 2019 Chinese Control Conference (CCC). IEEE Control Systems Magazine; 2019.
28. Tian W, Liu YJ, Liu B, et al. Guideline for thoracolumbar pedicle screw placement assisted by orthopaedic surgical robot. Orthop Surg, 2019, 11: 153–159.
29. Wallace SB, Cherkashin A, Samchukov M, Wimberly RL, Riccio AI. Real-time monitoring with a controlled advancement drill may decrease plunge depth. J Bone Joint Surg Am, 2019, 101: 1213–1218.
30. Dai Y, Xue Y, Zhang J. Noncontact vibration measurement based thoracic spine condition monitoring during pedicle drilling. IEEE/ASME Trans Mechatron, 2014, 19: 1532–1540.
31. Shao F, Bai H, Tang M, Xue Y, Dai Y, Zhang J. Tissue discrimination by bioelectrical impedance during PLL resection in anterior decompression surgery for treatment of cervical spondylotic myelopathy. J Orthop Surg Res, 2019, 14: 341.
32. Pohl BM, Jungmann JO, Christ O, Hofmann UG. Automated drill-stop by SVM classified audible signals. Annu Int Conf IEEE Eng Med Biol Soc, 2012, 2012: 956–959.
33. Klionsky DJ, Abdel-Aziz AK, Abdelfatah S, et al. Guidelines for the use and interpretation of assays for monitoring autophagy (4th edition)1. Autophagy, 2021, 17: 1–382.
34. Shao F, Tang M, Bai H, Xue Y, Dai Y, Zhang J. Drilling condition identification based on sound pressure signal in anterior cervical discectomy surgery. Med Sci Monit, 2019, 25: 6574–6580.
35. Dai Y, Xue Y, Zhang J. Condition monitoring based on sound feature extraction during bone drilling process. In: Control Conference. IEEE, 2014; 7317–7322.
36. Hirano Y, Ohara Y, Mizuno J, Itoh Y. History and evolution of laminoplasty. Neurosurg Clin N Am, 2018, 29: 107–113.
37. Tsuji H. Laminoplasty for patients with compressive myelopathy due to so-called spinal canal stenosis in cervical and thoracic regions. Spine (Phila Pa 1976), 1982, 7: 28–34.
38. Hirabayashi K, Miyakawa J, Satomi K, Maruyama T, Wakano K. Operative results and postoperative progression of ossification among patients with ossification of cervical posterior longitudinal ligament. Spine (Phila Pa 1976), 1981, 6: 354–364.
39. Hirabayashi K, Watanabe K, Wakano K, Suzuki N, Satomi K, Lshii Y. Expansive open-door laminoplasty for cervical spinal stenotic myelopathy. Spine (Phila Pa 1976), 1983, 8: 693–699.